Electromagnetic modeling of the CSNS H^- ion source extraction system

WU Xiao-Bing(吴小兵) OUYANG Hua-Fu(欧阳华甫)

Institute of High Energy Physics, Chinese Academy of Sciences, Beijing 100049, China

Abstract: A Penning surface H^- ion source test stand has been developed for the China Spallation Neutron Source (CSNS) at the Institute of High Energy Physics (IHEP). H^- beams with a current up to 50 mA and a pulse length up to 520 μs at a repetition rate of 25 Hz are obtained at present. In order to improve the extraction system based on both the results of the emittance measurements in experiment and the simulation results of the effect of the extraction system on the beam emittance, three dimensional electromagnetic finite element analysis and particle tracking are undertaken. First, the magnetic field of the deflecting magnet is studied in detail, and then the effect of the extraction geometry on the beam transport is also investigated.

Key words: CSNS, electromagnetic, particle tracking, beam transport

PACS: 29.20.Ej, 29.25.Ni **DOI:** 10.1088/1674-1137/36/4/014

1 Introduction

The CSNS is an accelerator-based high power project currently under R&D in China [1]. The accelerator complex consists of an 81 MeV H^- linear accelerator as an injector and a 1.6 GeV rapid cycling proton synchrotron. The linear accelerator consists of a 50 keV H^- Penning surface plasma ion source, a low energy beam transport line, a 3.0 MeV radio frequency quadrupole (RFQ) accelerator, a medium energy beam transport line, an 81 MeV drift tube linear accelerator and a high energy beam transport line. The H^- ion source is chosen to be of the Penning type, which is the same as the source for the ISIS [2–4]. At present, the construction of the CSNS H^- ion source test stand is finished and commissioning is in progress. Some results were described previously in detail [5].

The model of the CSNS H^- ion source extraction system, as shown in Fig. 1, includes an aperture plate (plasma electrode), an extraction electrode, a deflecting magnet and a post acceleration electrode. The beam is firstly extracted from the discharge chamber through a slit of 10 mm×0.6 mm in size on the aperture plate by the extraction field. The shape of the standard extraction electrode is a kind of long and narrow structure with an open ended jaw and a 13.2 mm×1.0 mm slit. The distance from the aperture plate to the extraction electrode is 1.94 mm and the applied extraction voltage between them is 17 kV. After extraction, the beam is bent through a 90° deflecting magnet (with a field gradient index of n=1) mounted in a refrigerated cold box [3]. There are three main purposes of the deflecting magnet and the cold box: (1) to analyze out the electrons extracted with the H^- ions; (2) to focus the beam profile from 10 mm×0.6 mm at the aperture to about 10 mm×10 mm at the cold box exit; and (3) to trap cesium vapor escaping from the source. The H^- ion beam emerges from a hole in the cold box and is further accelerated to 50 keV through a 60 mm post acceleration gap with a voltage of 33 kV.

2 Magnetostatics modeling

To study the effect of the magnetic field on the beam transport, the magnetic field is firstly studied and solved accurately. A three dimensional finite element analysis code has been used for the simulation. As shown in Fig. 1, the magnet yoke, the pole and the magnet coil are all included in the model. A regular hexahedral mesh is adopted for the magnetostatics solver. For a computer with 4 giga bytes (GB) random access memory (RAM), a total of approximately 4.5×10^6 mesh cells are available. Therefore a subtle balance on the mesh cell distribution between various

Received 6 July 2011

parts of the model is needed to ensure that the field is solved accurately. Because of the vast difference in scales among the extraction, deflecting and post acceleration region, mesh cell densities vary from 1×10^{8} to 2×10^{13} m^{-3}.

Theoretically, for the H^- beam with energy of 17 keV, a deflecting field of 2353 Gs is required to bend the beam along a circular trajectory with a radius of 80 mm. Then, the magnet coil current can be also calculated based on the field through the simulation. In Fig. 2, the relationships between the magnetic field and the coil current obtained by simulations, measurements and experiments are shown.

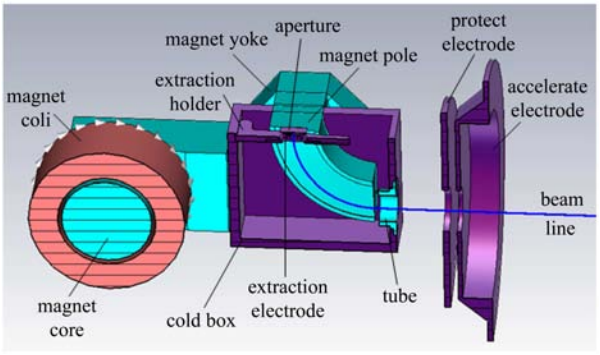

Fig. 1. Model of the CSNS H^- ion source extraction system.

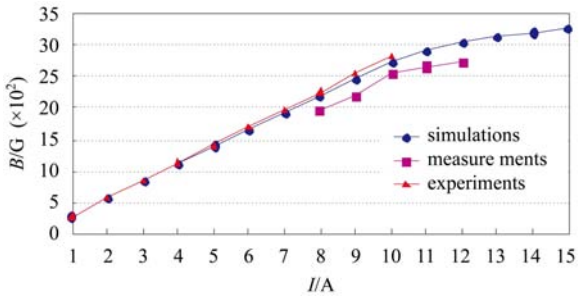

Fig. 2. Variation of the magnetic field with the coil current.

As shown in Fig. 2, the magnetic field of 2353 Gs is corresponds to a current of 8.6 A obtained by the simulation (dot), 8.3 A by the experiment (triangle) and 9.5 A by the measurement (square). The coil current obtained by the experiment is a little bit smaller than that by the simulation, and it should be due to errors produced during manufacture and installation. It is estimated that the magnetic field deviation is in an order of 20 Gs per 0.1 mm of the gap deviation between the magnet poles. However, the measured current is much larger than those obtained by the other two methods. It may be due to the rough measurement method of using a Hall coil and without precise positioning. In addition, it can be seen in the figure that when the coil current is smaller than 11 A, the magnetic field varies sharply and almost linearly with the coil current. When the coil current is larger than 11 A, the magnetic field varies smoothly and nears saturation.

The magnetic field distribution along the beam line for the 17 keV H^- ion beam is shown in Fig. 3. As shown in the figure, the magnetic field is basically uniform in the deflecting magnet region with a value of 2353 Gs. The magnet fringe field also exists at both the entrance and the exit of the magnet for the finite length of the deflecting magnet. While the magnet fringe field at the entrance side is beneficial for the Penning discharge, the magnet fringe field at the exit side is harmful to the beam transport downstream. It will cause the beam center to deviate from the beam line in the vertical direction. To overcome this effect, a tube made of the material with high permeability, which is the same as the magnet pole, is inserted into the fringe field region. The contour line of the magnetic field is shown in Fig. 4.

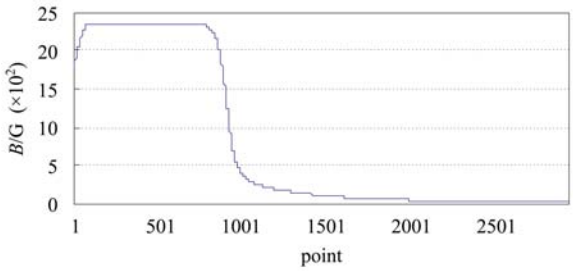

Fig. 3. Magnetic field distribution along the beam line.

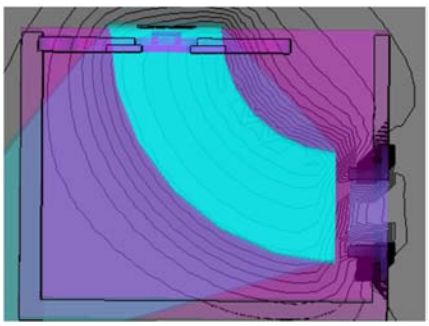

Fig. 4. Magnetic field contour line of the deflecting magnet.

From Fig. 4, it can be seen that the density of the contour line is not uniform in the radius direction because the field gradient index of n=1. The magnetic field at the exit of the deflecting magnet is terminated by the insertion of the tube. As is known,

when the field gradient index of n <1, the beam undergoes weak focusing in both the radius direction and its vertical direction. When n >1, the beam undergoes strong defocusing in the radius direction and strong focusing in its vertical direction. Only when n=1, the parallel beam can be transported along the beam line without consideration of the space charge force [6]. The distribution of the magnetic field gradient index n in the radius direction is shown in Fig. 5. The average of n is 1.11, which is larger than 1.

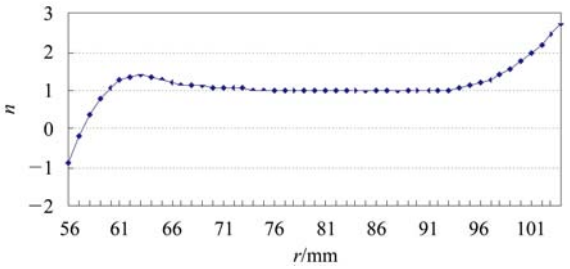

Fig. 5. Variation of the magnetic field gradient index n with the radius r.

As shown in Fig. 5, the magnetic field gradient index n is almost uniform with n=1 in the range of the radius from 74 to 94 mm. This region is the good field region. However, when the radius is smaller than 74 mm and larger than 94 mm, the magnetic field gradient index n is severely deviates from 1 due to the shims at the magnet profile ends.

3 Particle tracking

After the electromagnetic fields are calculated, particles representing the H$^-$ ions are tracked through the particle tracking mode. The particle tracking mode includes a magnetostatic solver, an electrostatic solver and a particle tracking solver. First, the particle tracking solver simply computes the trajectory of the particle through a pre-calculated electromagnetic field by using the magnetostatic solver and electrostatic solver, then a self-consistent gun-iteration is used. The gun-iteration consists of an iterative application of an electrostatic solver and a particle tracker. More than 1×10^4 macro particles with uniform thermal energy and a random uniform spatial distribution are emitted from the slit on the aperture plate orthogonally [2]. Although the simulations of the H$^-$ beam with different currents and different space charge neutralization are carried out, as a typical example, only the simulation results of H$^-$ beam with a current of 100 mA and 90% space charge neutralization are presented here. A particle monitor is set up to monitor the beam profile, and the horizontal and vertical emittance along the beam line. The simulation results are shown in Fig. 6.

As can be seen from Fig. 6(a), the beam profile is almost symmetrical about both the x and y axes.

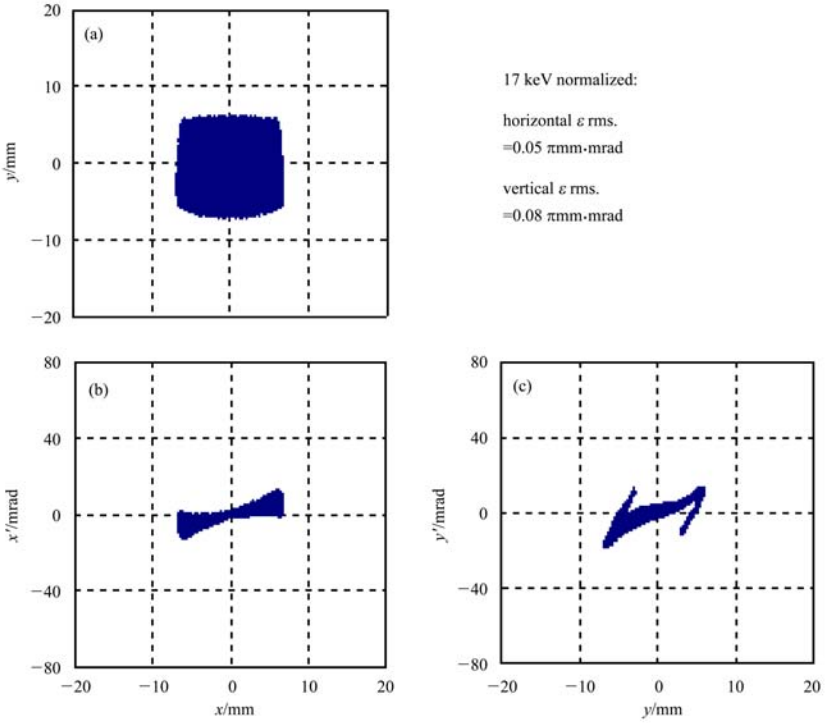

Fig. 6. Particle distribution at the exit of the cold box, (a) beam profile, (b) particle distribution in horizontal phase space, and (c) particle distribution in vertical phase space.

However, as shown in Fig. 6(c), there is an aberration in the vertical phase space. As will be seen from the following simulation results. This is caused by the open ended jaw of the standard extraction electrode. The normalized root mean square emittances of the horizontal and vertical are also not equal to each other due to the aberration in the vertical phase space. In Fig. 7, the standard extraction electrodes and Pierce extraction electrodes [7] are shown. There are also two geometric shapes, the open and the terminated, for both kinds of electrode.

Simulations are carried out to investigate the effect of the terminated geometric shape of the standard extraction electrode as the second geometry shown in Fig. 7. The results are shown in Fig. 8.

As shown in Fig. 8, the terminated geometry of the extraction electrode produces a beneficial effect. The aberration in the focusing has disappeared from the vertical phase space. The normalized root mean square emittances of the horizontal and vertical are also equal to each other. Simulations are also carried out to investigate the Pierce extraction electrode with the terminated geometry. The results are shown in Fig. 9.

As shown in Fig. 9, the beam profiles are both symmetric in the horizontal and vertical planes. The normalized root mean square emittances of the horizontal and vertical planes are also equal to each other, and the value is a bit smaller than the standard geometry.

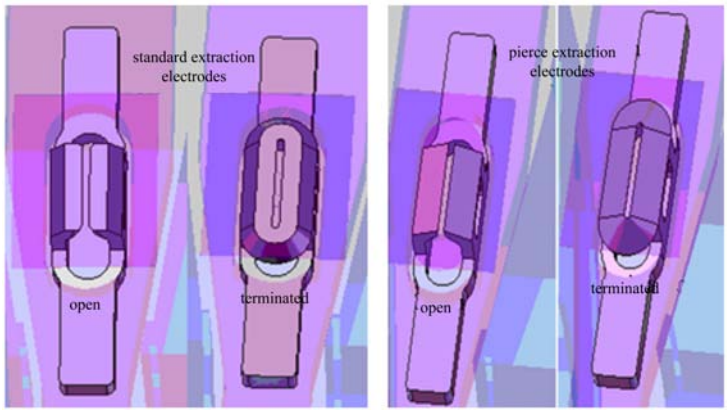

Fig. 7. Model of the extraction electrode geometries.

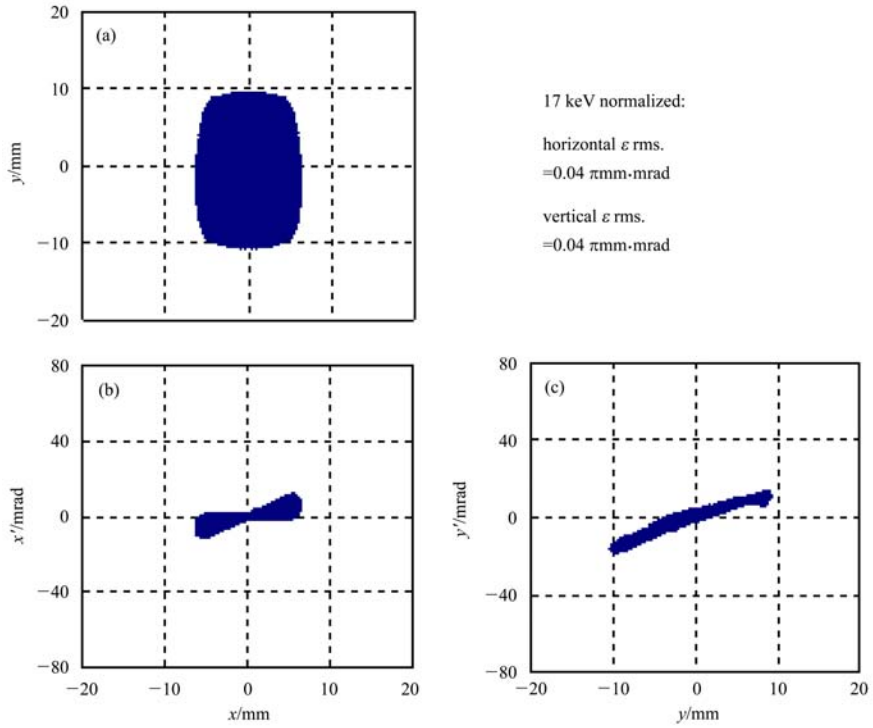

Fig. 8. Particle monitors at the exit of the cold box with a terminated extraction electrode.

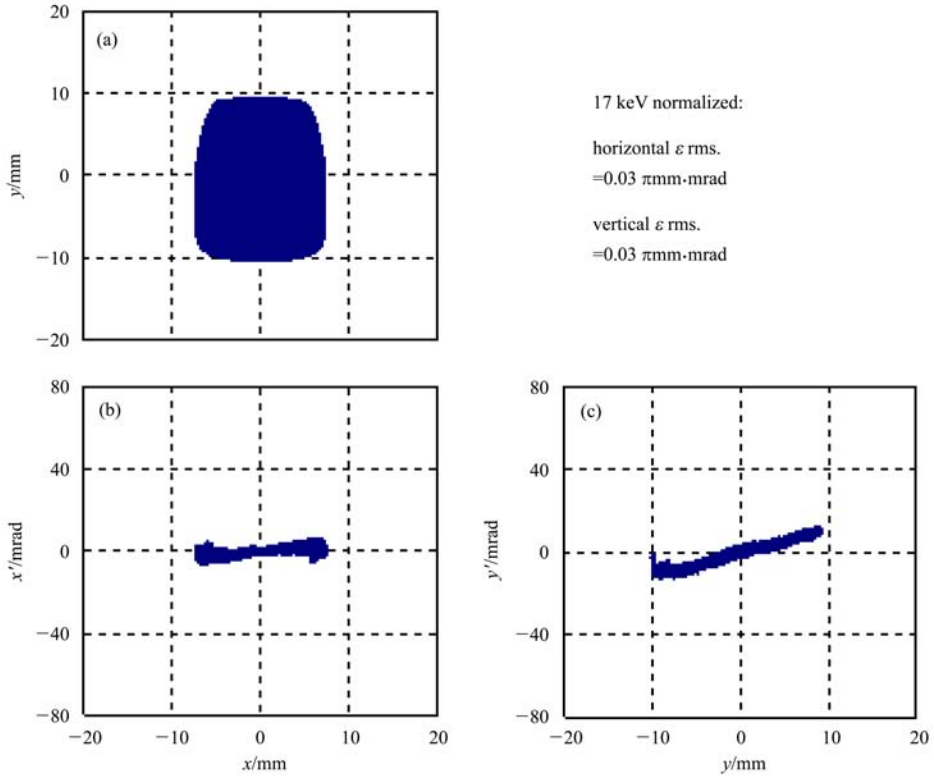

Fig. 9. Particle monitors at the exit of the cold box with a terminated extraction electrode.

4 Conclusion

The magnetostatics field calculation is used, and the results are well applied in experiment. The particle tracking of the ion source extraction has demonstrated that the terminated geometry of both the standard and Pierce extraction electrode has a beneficial effect for the H$^-$ ion beam. The aberration of the vertical plane has been removed, and the normalized root mean square emittances of the horizontal and vertical planes become equal to each other. Although the effects predicted by the finite element analyzing may be idealized. It is still expected that this work will have a significant impact on improving the CSNS ion source. Tests with these geometric changes will be incorporated into experiments on the CSNS ion source test stand in the near future. Optimizations of the beam transport in the deflecting magnet and the post acceleration region are predicted to have a beneficial effect on the beam performances [6, 8, 9].

References

1 WEI J, FU S N, TANG J Y. Chinese Physics C (HEP & NP), 2009, **33**(11): 1033–1042
2 Faircloth D C, Thomason J W G, Whitehead M O. Review of Scientific Instruments, 2004, **75**(5): 1735–1737
3 Faircloth D C, Letchford A P, Gabor C et al. Review of Scientific Instruments, 2008, **79**(2): 02B717
4 Faircloth D C, Lawrie S, Letchford A P et al. Review of Scientific Instruments, 2010, **81**(2): 02A721
5 WU X B, OUYANG H F, CHI Y L et al. Chinese Physics C (HEP & NP), 2011, **35**(7): 679–683
6 Lawrie S R, Faircloth D C, Letchford A P. Modifications to the Analysing Magnet in the ISIS Penning Ion Source. In: Proceedings of EPAC. Genoa: Perir-Jean-Genaz C, 2008. 427–429
7 Pierce J R. Theory and Design of Electron Beams. 2nd ed. New York: Van Nostrand, 1954
8 Lawrie S R, Faircloth D C, Whitehead M O et al. AIP Conference Proceedings, 2009, **1097**(1): 253–262
9 Faircloth D C, Whitehead M O, Wood T W. Study of the Post Extraction Acceleration Gap in the ISIS H$^-$ Penning Ion Source. In: Proceedings of EPAC. Genoa: Perir-Jean-Genaz C, 2008. 406–408